



## Synthesis, characterization and electrocatalytical behavior of Nb–TiO<sub>2</sub>/Pt nanocatalyst for oxygen reduction reaction

N.R. Elezović<sup>a</sup>, B.M. Babić<sup>b</sup>, Lj. Gajić-Krstajić<sup>c</sup>, V. Radmilović<sup>d</sup>, N.V. Krstajić<sup>e</sup>, L.J. Vračar<sup>e,\*</sup>

<sup>a</sup> Institute for Multidisciplinary Research, Belgrade, Serbia

<sup>b</sup> Vinča Institute of Nuclear Sciences, Belgrade, Serbia

<sup>c</sup> Institute of Technical Sciences-SASA, Belgrade, Serbia

<sup>d</sup> National Center for Electron Microscopy, LBLN University of California, Berkeley, USA

<sup>e</sup> Faculty of Technology and Metallurgy, University of Belgrade, Belgrade, Serbia

### ARTICLE INFO

#### Article history:

Received 14 September 2009

Received in revised form 11 January 2010

Accepted 17 January 2010

Available online 28 January 2010

#### Keywords:

Nb–TiO<sub>2</sub> support

Nb–TiO<sub>2</sub>/Pt catalyst

Oxygen reduction reaction

Methanol

### ABSTRACT

In order to point out the effect of the support to the catalyst for oxygen reduction reaction nano-crystalline Nb-doped TiO<sub>2</sub> was synthesized through a modified sol–gel route procedure. The specific surface area of the support,  $S_{\text{BET}}$ , and pore size distribution, were calculated from the adsorption isotherms using the gravimetric McBain method. The support was characterized by X-ray diffraction (XRD) technique.

The borohydride reduction method was used to prepare Nb–TiO<sub>2</sub> supported Pt (20 wt.%) catalyst. The synthesized catalyst was analyzed by TEM technique.

Finally, the catalytic activity of this new catalyst for oxygen reduction reaction was investigated in acid solution, in the absence and the presence of methanol, and its activity was compared towards the results on C/Pt catalysts.

Kinetic analysis reveals that the oxygen reduction reaction on Nb–TiO<sub>2</sub>/Pt catalyst follows four-electron process leading to water, as in the case of C/Pt electrode, but the Tafel plots normalized to the electrochemically active surface area show very remarkable enhancement in activity of Nb–TiO<sub>2</sub>/Pt expressed through the value of the current density at the constant potential.

Moreover, Nb–TiO<sub>2</sub>/Pt catalyst exhibits higher methanol tolerance during the oxygen reduction reaction than the C/Pt catalyst.

The enhancement in the activity of Nb–TiO<sub>2</sub>/Pt is consequence of both: the interactions of Pt nanoparticles with the support and the energy shift of the surface d-states with respect to the Fermi level what changes the surface reactivity.

© 2010 Elsevier B.V. All rights reserved.

### 1. Introduction

In spite of the experimental and theoretical progress, many questions still remain unsolved related to the low temperature fuel cell systems, e.g., the polymer electrolyte membrane fuel cell (PEMFC) or the direct methanol fuel cell (DMFC).

Highly irreversible oxygen reduction as cathodic reaction in the cell that exhibits slow kinetic behavior is a problem in term of efficiency of the fuel cell [1,2], since the onset potential of the oxygen reduction at practically working current densities is about 0.4 V below the reversible thermodynamic potential of 1.23 V. Another crucial problem in the DMFC technology is methanol crossover from the anode to the cathode side through the polymer electrolyte

membrane, leading to potential loss and additional reduction in efficiency. One of the routes dealing with these problems is the development of good catalyst that will, at the same time, have high methanol tolerance. To avoid methanol crossover problem the relevant proton exchange membranes [3] should be developed, too.

Despite all the efforts to find replacements, platinum and platinum alloys are the best known electrocatalytic materials for oxygen reduction reaction [4–6], since they have the best activities and chemical stability, but the problem is high costs of Pt loadings in operating cathodes. Incorporation of some transition metals (Ru, Rh, Ir) into Pt is found to improve activity for methanol oxidation but there is no unique conclusion when oxygen reduction is concerned [7–10]. According to some studies they reduce Pt activity, but the other stated that by replacing part of Pt monolayer with transition metal enhanced the activity compared to the pure Pt, and that was explained by the reduction of OH coverage on Pt at low potentials according to the stronger adsorption of OH on them then on pure Pt [11]. Dissolution of some other transition metals (Ni, Co, Fe) was unfortunately noticed, on the other hand, that low-

\* Corresponding author at: Faculty of Technology and Metallurgy, University of Belgrade, Physical Chemistry and Electrochemistry, Karnegijeva 4, Belgrade 11000, Serbia. Tel.: +381 113303685; fax: +381 113370387.

E-mail address: [ljvracar@tmf.bg.ac.rs](mailto:ljvracar@tmf.bg.ac.rs) (L.J. Vračar).

ers stability of the catalyst the factor that must be considered for the catalyst, as well. The oxygen reduction on the platinum is a structure sensitive reaction and the activity of the surface generally increases as the surface area decreases. The reason for the activity differences is variation of the different Pt crystal planes exposed to the electrolyte as a function of the particle size [12,13]. The effect of the particle size on OOR for carbon-supported Pt high surface area catalyst in kinetic region that shows the trend of increasing specific activity with increasing particle size was analyzed in the literature [14]. The increase of Pt particle size reduces the energy of adsorbed oxygen species that facilitates the reduction of these species leaving more Pt sites available for the oxygen reduction.

The supporting material for the functioning of the catalysts is very important, as well, and it should be a good combination of excellent electronic conductivity and good corrosion resistivity. Carbon or graphite is the most widely used catalyst support as it provides good electronic conductivity, on one hand, and physical surface for dispersion of small Pt particles that is necessary to achieve high surface area, on the other hand, diminishing the catalyst loading, too. However, carbon corrosion reaction could be provoked by start/stop of a simple fuel cell [15] or since the oxygen reaction is very irreversible, carbon corrosion could proceed during recharge of the regenerative fuel cell at the air electrode, at high potentials. This could damage the carbon support and the cell performance, as well. That is why other support catalysts have recently become available as a nonstoichiometric mixture of several titanium oxide phases, mainly  $Ti_4O_7$  and  $Ti_5O_9$ , known as Magneli phases, whose registered name is Ebonex [16–18]. Ebonex is electrochemically stable, with very high overpotentials for hydrogen and oxygen evolutions, in acid and base solutions, and high electrical conductivity of  $10^3 \Omega^{-1} \text{cm}^{-1}$ , too, and that is why it could be suitable as catalyst support material. According to the Brewer theory [19], since Ebonex is reduced titania and has hypo-d-electron character it is expected to have an ability to interact with inert noble metals, like platinum, changing additionally the catalytic activity of the platinum. This change in catalytic activity could also be explained taking into the consideration Hammer and Norskov concept [20] of the metal reactivity changes, through the changes in adsorbate–surface interaction energy due to the move of the local d-bond position relative to the Fermi level.

Recently we have synthesized Pt catalyst using Ebonex as a support and found the enhancement of the catalytic activity towards oxygen reduction that was very evident through the change of electrochemically active surface area and enhancement of activity, in comparison with polycrystalline Pt, expressed through the specific current densities obtained at the constant potential [21]. We concluded that better catalytic efficiency for oxygen reduction was caused by facilitation of  $O_2$  interactions with the adsorption sites (so-called active sites) on the surface of the catalyst indicating that the interplay of the electronic and geometric factors affected the decrease of OH chemisorption and increase kinetics of oxygen reduction.

However, the main disadvantage of sub-stoichiometric titanium oxides as supporting material is very low specific surface area. The maximum value that can be achieved is around of  $15 \text{ m}^2 \text{ g}^{-1}$ , even after ball-milling that prevents achieving a high dispersion and compositional homogeneity of the catalyst clusters on a support, which is important requirement for an enhanced electrocatalytic activity.

The literature findings demonstrate that niobium oxide nanoparticles can be adequate support for Pt, as well, reducing further the noble-metal contents of catalyst for oxygen reduction. Since niobium oxides have excellent chemical stability in acid solutions they could diminish the problems of the substrate oxidation and corrosion degradation as in case of the pure carbon support [22].

It has also been reported that, when titania is doped with pentavalent impurity ions, i.e.,  $Nb^{5+}$ , these ions get into the anatase titania crystalline structure hindering its phase transformation to rutile and inhibiting grain growth. The effect is attributed to the extra valence of niobium ions, and that reduces oxygen vacancies in anatase phase inhibiting the transformation to rutile. Nb-doped titania used for gas sensor applications shows higher sensitivity towards oxygen and shorter response time than pure  $TiO_2$  [23].

Recently, Chen et al. [24] have found that Pt–Ir–Ru catalysts supported on rutile  $Nb_{0.1}Ti_{0.9}O_2$  have very good conductivity and better electrochemical stability in acid solution than the same catalyst supported on Ebonex, especially at high anodic potentials. Park and Seul [25] referred that  $NbTiO_2$  supported Pt catalyst showed an excellent catalytic activity for oxygen reduction mainly due to well dispersion of Pt on  $NbTiO_2$  until Ruiz et al. Ref. [26] suggested, too, that doping of  $TiO_2$  with Nb slows down the anatase to rutile phase transformation preventing growth of the grains, and that might lead to enhancement of the specific surface area of the support.

In the present study, we first synthesized nano-crystalline Nb-doped  $TiO_2$  support, and then, synthesized and physically characterized Pt catalyst supported on it. Finally, we investigated the catalytic activity of this new catalyst for oxygen reduction reaction, in acid solution, in the absence and the presence of methanol, and compared its catalytic activity towards ORR with results on C/Pt catalyst and discussed it in relation to the other findings in the literature [14,25,27–30].

## 2. Experimental

### 2.1. Preparation of Nb-doped $TiO_2$ support

*Nb-doped  $TiO_2$  nanosized powder was synthesized through modified sol–gel procedure proposed by Boujday et al. [31]. The procedure considers acid-catalyzed sol–gel method in non-aqueous medium. Sol was prepared by adding volume of 0.9 ml of 37% solution of hydrochloric acid (Zorka, Serbia) to 40 ml of 97% solution of titanium tetraisopropoxide,  $Ti(OiPr)_4$  (Alfa Aesar, Germany), and an appropriate volume of 0.17 ml of 99.95% niobium(V) ethoxide (Aldrich, Germany) under vigorous stirring (0.5% Nb in Nb/Ti atomic ratio to get the  $Nb_{0.005}Ti_{0.995}O_2$  solid solution). Finally, 4.8 ml of deionized water was added under continuous stirring. Mixture was placed in glass tubes, sealed and placed at room temperature for 5 days. In the presence of such amount of hydrochloric acid, the hydrolysis proceeded without forming precipitate, leading to transparent sol. Gellification of the sol was achieved by adding an appropriate amount of water.*

The sample was dried by freeze-drying method using Modulyo Freeze Dryer System Edwards, England, consisting of freeze dryer unit at High Vacuum Pump E 2M 8 Edwards. Sample was pre-frozen in deep-freeze refrigerator at  $-30^\circ\text{C}$  for 24 h. After that, sample was frozen drying in the acrylic chamber with shelves arrangements mounted directly on the top of the condenser of freeze dryer. The vacuum during 20 h of freeze-drying was around 4 mbar.

Dried sample was heated to obtain anatase crystallized phase and to remove traces of organics in a conventional furnace, at  $400^\circ\text{C}$ , for 2 h. After the treatment, the furnace was cooled at room temperature. Finally, to activate Nb donor dopant in  $TiO_2$ , the nanoparticles were additionally annealed at  $400^\circ\text{C}$  for 2 h under pure  $H_2$  gas flow and cooled to room temperature under  $H_2$  gas atmosphere.

### 2.2. Synthesis of Nb– $TiO_2$ /Pt catalyst

The Nb– $TiO_2$  supported Pt (20 wt.%) catalyst ( $Nb_{0.005}Ti_{0.995}O_2$ /Pt) was prepared by means of borohydride

reduction method. Appropriate amount of  $\text{H}_2\text{PtCl}_6$  was dissolved in D.I. water. The Nb– $\text{TiO}_2$  support was dispersed in D.I. water and then mixed by adding metal salt solution with constant stirring. The mixture of metal salt and support was reduced by using excess of sodium borohydride solution. The precipitate was washed with D.I. water and then dried at  $80^\circ\text{C}$ .

The Pt/C catalyst with Pt loading of 20 wt.%, and specific surface area of Pt particles of  $96\text{ m}^2\text{ g}^{-1}$ , that is used as benchmark, was synthesized using modified ethylene glycol method on a home made carbon cryogel powder. The details of carbon support and C/Pt catalyst preparations are fully described in Refs. [32,33].

### 2.3. Cell and electrode preparation

Twenty milligrams of Nb-doped  $\text{TiO}_2/\text{Pt}$  catalyst was ultrasonically suspended in 9.5 ml of water and 0.5 ml of Nafion solution (5 wt.% Aldrich solution) to prepare catalyst ink. Then, 20 (l of ink was transferred with an injector to a gold disk electrode (6 mm diameter, with area of  $0.28\text{ cm}^2$ ). After the water volatilization, the electrode was heated at  $80^\circ\text{C}$  for 10 min. For all electrodes, the Pt loading was 8 (g of Pt. A conventional RDE three-compartment cell was used. The working electrode compartment was separated from other two compartments by fritted glass discs. The counter electrode was platinum sheet of  $5\text{ cm}^2$  geometric area. All measurements were done with Pt/ $\text{H}_2$  reference electrode (RHE) in the same solution at the same temperature as working electrode. The RHE was kept in compartment separated from the working electrode by wetted closed glass stopcock and  $\text{H}_2$  purified gas was bubbled continuously through the solution. The potential of RHE was checked with saturated calomel electrode.

### 2.4. Electrode characterization

#### 2.4.1. Adsorption and desorption isotherms

Adsorption and desorption isotherms of  $\text{N}_2$  were measured on Nb– $\text{TiO}_2$  support at  $-196^\circ\text{C}$ , using the gravimetric McBain method. The specific surface area,  $S_{\text{BET}}$ , and pore size distribution, were calculated from the isotherms. Pore size distribution was estimated by applying BJH method [34] to the desorption branch of isotherms.

#### 2.4.2. XRD analysis

Structural analysis (XRD) was carried out by Siemens D-500 diffractometer.  $\text{Cu K}\alpha$  radiation was used in conjunction with a  $\text{Cu K}\beta$  nickel filter. XRD was used to evaluate the crystallite size of the Nb– $\text{TiO}_2$  support. The average crystallite size,  $D$ , was calculated from Scherrer's formula:  $D = 0.9\lambda / \beta \cos\theta$ , where  $\lambda$  is the wavelength of the X-rays,  $\theta$  is the diffraction angle,  $\beta = (\beta\text{m}^2 - \beta\text{s}^2)$ ,  $\beta$  is corrected half-width,  $\beta\text{m}$  observed half-width and  $\beta\text{s}$  is half-width of the standard Si sample (provided by Siemens).

#### 2.4.3. TEM measurements

Transmission electron microscopy (TEM) measurements were performed at the National Center for Electron Microscopy (NCEM-Berkeley) using the FEI (Fillips electronic instruments)-CM200 super-twin and CM300 ultra-twin microscopes operating at 200 and 300 kV and equipped with the Gatan  $1\text{ k} \times 1\text{ k}$  and  $2\text{ k} \times 2\text{ k}$  CCD cameras, respectively. Specimens were prepared for transmission electron microscopy by making suspensions of the catalyst powder in ethanol, using an ultrasonic bath. These suspensions were dropped onto clean holey carbon grids, which were then dried in the air.

Particle size distribution was determined from images of, on average, 20 different regions of the catalyst; each region contained 10–20 particles. The particle shapes were determined by real space crystallography with the use of high-resolution images taken from particles near or on the edge of the Nb– $\text{TiO}_2$  substrate, and/or by

numerical Fourier filtering of the digitized image intensity spectrum of particles on top of the carbon.

#### 2.4.4. Electrochemical characterization

The cyclic voltammetry experiments were performed in the potential range between hydrogen and oxygen evolution, in  $0.5\text{ mol dm}^{-3}$   $\text{HClO}_4$  solution, with various scan rates at rotating speed of 2500 rpm, at Nb– $\text{TiO}_2/\text{Pt}$  and C/Pt electrodes. The solution ( $\text{HClO}_4$  Spectrograde, Merck) was prepared in deionized water ("Millipore"  $18\text{ M}\Omega$ ), at the temperature of  $25^\circ\text{C}$ , and it was saturated with high purity nitrogen that was continuously bubbling through the working electrode compartment.

The experiments were done by potentiodynamic method. A PAR Universal Programmer-Model 175 was used to provide potentiodynamic voltage time program addressed to PAR Model 371 Potentiostat/Galvanostat.

## 3. Results and discussion

### 3.1. BET, XRD analysis of Nb– $\text{TiO}_2$ support

Nitrogen adsorption isotherm for support that was classified, according to the IUPAC classification [35], as type IV with hysteresis loop which is associated with mesoporous materials—is presented at Fig. 1(a). Specific surface area of Nb– $\text{TiO}_2$  powder calculated by BET equation was determined to be  $72\text{ m}^2\text{ g}^{-1}$ . The pore size distribution (Fig. 1(b)) has a sharp peak and the values of the pore radius for the maximum of observed curve was found to be 2–4 nm.

X-ray pattern of sample (Fig. 2) shows that all peaks belong to the anatase phase and any niobium compound is not detected. Broad peaks indicate the nano size of particles. Calculated average particle size is 13 nm. The lattice parameters are  $a = b = 0.37854\text{ nm}$  and  $c = 0.94835\text{ nm}$ . Our anatase has enlarged lattice parameters compared with pure anatase (JCPDS 21-1272) and that indicates that niobium is incorporated into the lattice.

### 3.2. TEM analysis of Nb– $\text{TiO}_2/\text{Pt}$ catalyst

Fig. 3(a) shows low-magnification transmission electron micrographs of Pt catalyst supported on Nb– $\text{TiO}_2$ . This image shows that the Pt nanoparticles are globular in shape and reasonably uniformly distributed over Nb– $\text{TiO}_2$  support and that is why it was possible to determine Pt particle size distribution and to calculate the total surface area of the particles by analysing different region of the catalyst from images. The high-resolution electron microscopy image of the Pt catalyst on Nb– $\text{TiO}_2$  is shown in Fig. 3(b). Catalyst sample shows mono-modal particle size distribution (Fig. 3(c)) with mean particle sizes of 3.5 nm.

### 3.3. Cyclic voltammetry results

The cyclic voltammetric response of Nb– $\text{TiO}_2$  support was first analyzed in the potential range between oxygen and hydrogen evolution in  $0.5\text{ mol dm}^{-3}$   $\text{HClO}_4$  solution. The CV-curve (Fig. 4(a)) shows the rectangular shape that is expected for an ideal electrochemical double-layer capacitor and does not show any significant peaks revealing the presence of oxidative–reductive processes. A good conductive support material for bifunctional catalyst such in metal–air batteries, should be characterized by poor electroactivity for hydrogen evolution, as it could occur during cell discharge causing overpressure in the cell. This result proves that Nb– $\text{TiO}_2$  is highly conductive and electrochemically inert material in the whole range of potential [0.03–1.30 V(RHE)]. The CV-curve of Nb– $\text{TiO}_2/\text{Pt}$  (8 (g) sample (Fig. 4(b)), (the loadings of Nb– $\text{TiO}_2$  in (a) and (b) are the same), in the same solution saturated with  $\text{N}_2$ , represents typical voltammogram of Pt with very clear hydrogen

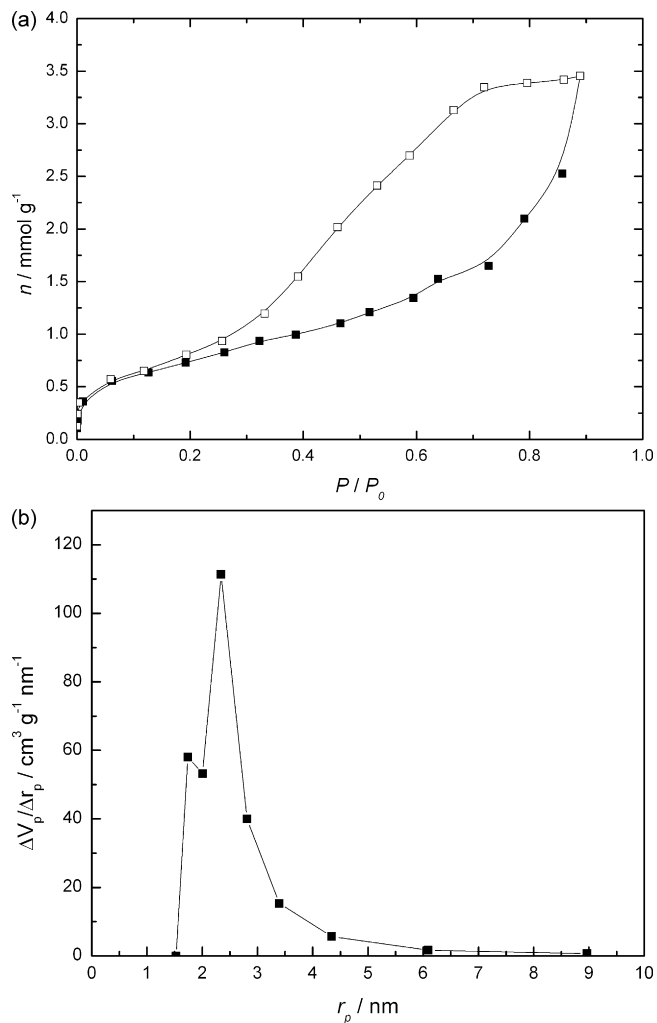


**Fig. 1.** (a) Nitrogen adsorption isotherm, as the amount of N<sub>2</sub> adsorbed as a function of relative pressure for Nb-TiO<sub>2</sub> substrate. Adsorption—solid symbols, desorption—open symbols and (b) pore size distribution of Nb-TiO<sub>2</sub>.

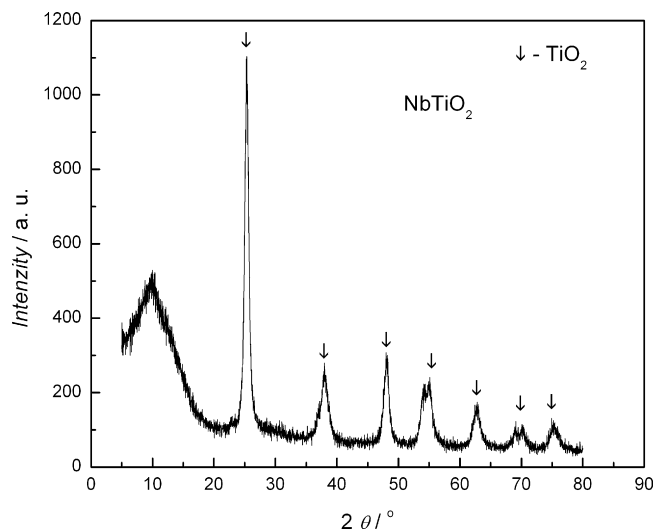


**Fig. 2.** X-ray diffraction spectra of Nb-TiO<sub>2</sub> substrate with specified composition.

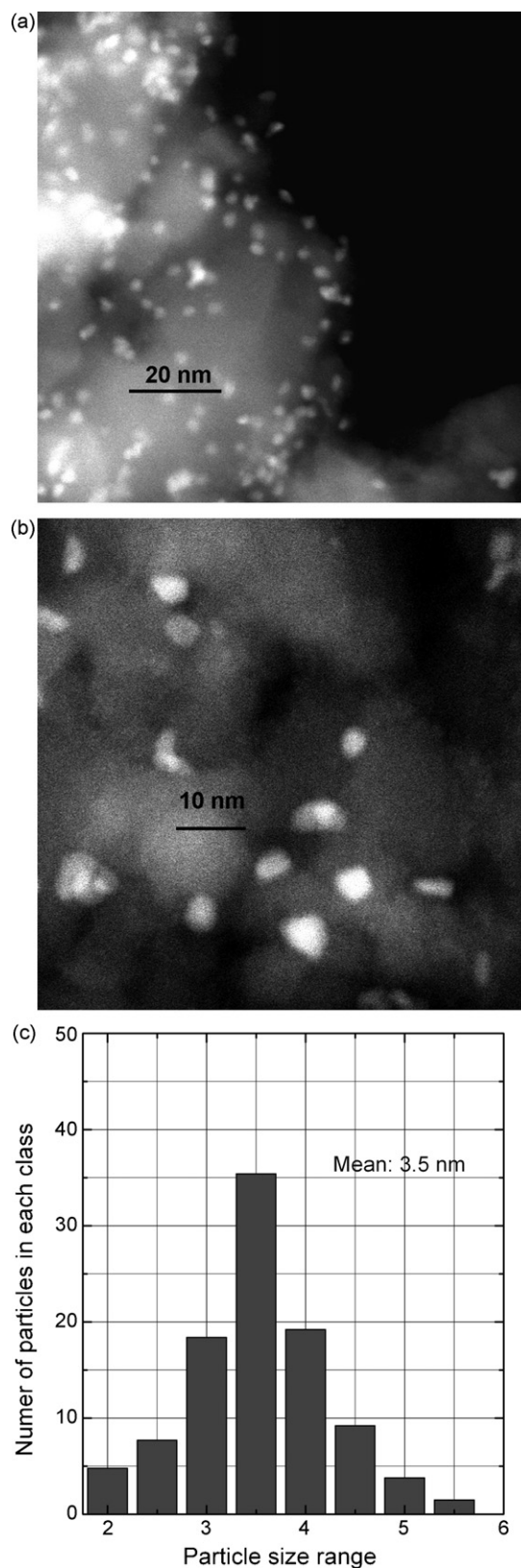


**Fig. 3.** TEM images of Pt nanoparticles on Nb-TiO<sub>2</sub> substrate: (a) low-magnification overview showing the spread of the Pt particles distribution on Nb-TiO<sub>2</sub> support; (b) high-resolution image showing no evidence for pronounced particles agglomeration; (c) Pt particle size distribution obtained from the micrograph obtained from (a).

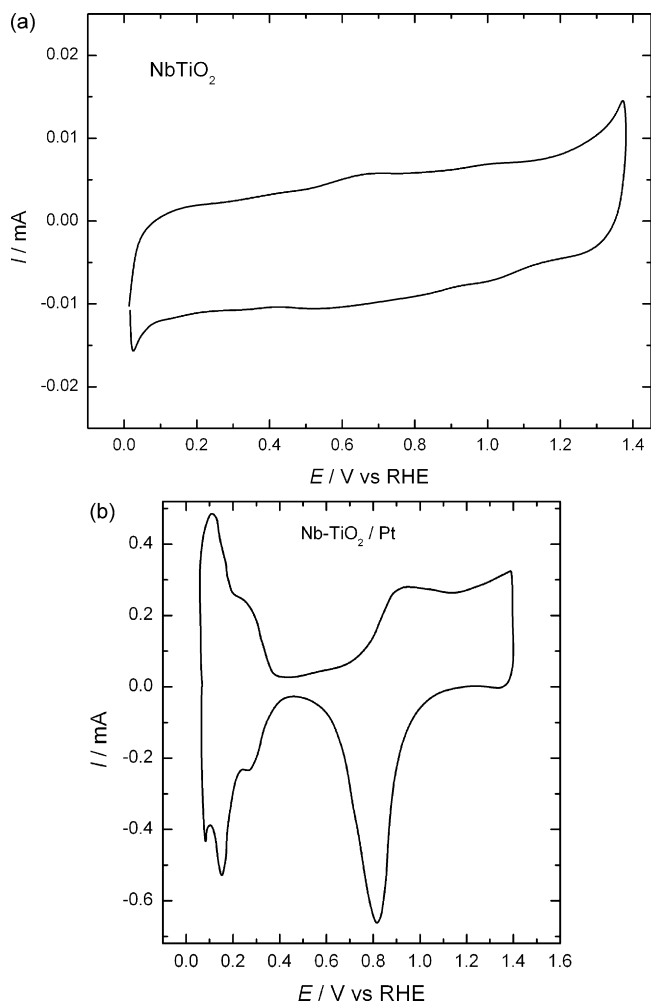


**Fig. 4.** Cyclic voltammograms for: (a) Nb-TiO<sub>2</sub> substrate and (b) Nb-TiO<sub>2</sub>/Pt (8 μg) electrode, (the loadings of Nb-TiO<sub>2</sub> in (a) and (b) are the same), with sweep rate of 100 mV s<sup>-1</sup>, in N<sub>2</sub> saturated 0.5 mol dm<sup>-3</sup> HClO<sub>4</sub> solution.

adsorption/desorption and PtOH formation and reduction regions, with well defined cathodic peak at 0.80 V (RHE), observed during the reduction potential scan that represents reduction of oxygen adsorbed species.

Electroactive surface area of Pt was determined from adsorption/desorption charge of hydrogen atoms, after double-layer charge subtraction, taking the reference value of 210 (C cm<sup>-2</sup>) as a charge of full coverage with adsorbed hydrogen species [36]. This calculation gives the value of specific electroactive area of 42.5 m<sup>2</sup> g<sup>-1</sup> (Pt) for Nb-TiO<sub>2</sub>/Pt (8 g) electrode.

Geometric surface area of Pt catalyst particles calculated from average diameter is 79.9 m<sup>2</sup> g<sup>-1</sup>. This value is significantly higher than active surface area obtained from cyclic voltammetry. However, brief inspection of TEM images undoubtedly shows the presence of some agglomerated Pt particles beside well dispersed, leading to low utility efficiency of catalyst.

#### 3.4. Oxygen reduction on Nb-TiO<sub>2</sub>/Pt catalyst

To test the behaviour of the Nb-TiO<sub>2</sub>/Pt as a catalyst for oxygen reduction reaction, in comparison with the pure C/Pt, the rotating disk electrode measurements were done in O<sub>2</sub> saturated HClO<sub>4</sub> solution, with the sweep rate of 20 mV s<sup>-1</sup> (Fig. 5). These results clearly show that the onset of O<sub>2</sub> reduction is significantly (about 80 mV) shifted to the positive potentials for Nb-TiO<sub>2</sub>/Pt electrode with reference to that obtained with C/Pt. The remarkable activity is

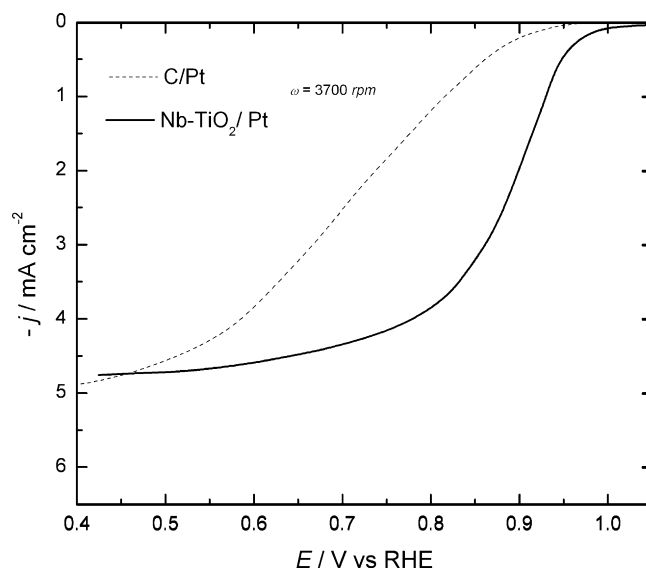


**Fig. 5.** Polarization curves (positive-going sweeps) of a prepared Nb-TiO<sub>2</sub>/Pt (8 μg) and C/Pt (8 μg) catalysts in 0.5 mol dm<sup>-3</sup> HClO<sub>4</sub> solution saturated with oxygen at a scan rate of 20 mV s<sup>-1</sup> and rotation rate of 3700 rpm. Current densities are normalized to the geometric surface area.

explained by half-wave potential that is 0.88 V (RHE) at Nb-TiO<sub>2</sub>/Pt comparing to the 0.70 V (RHE) at C/Pt which indicates its excellent catalytic activity for the reduction of oxygen. These results do not correlate with CV results that showed the lower real active surface area for Nb-TiO<sub>2</sub>/Pt determined from hydrogen UPD region, but they clearly suggest very significant increase of the number of active Pt sites for Nb-TiO<sub>2</sub> as a support, probably through the change of electronic structure of the catalyst, connected to the interactions between platinum and the supportive material.

The polarization curves for oxygen reduction of the Nb-TiO<sub>2</sub>/Pt at various rotating speeds from 400 to 3700 rpm with scan rate of 20 mV s<sup>-1</sup> in 0.5 mol dm<sup>-3</sup> HClO<sub>4</sub> are shown in Fig. 6(a).

For oxygen reduction as a mixed control process, the activation and mass-transport-controlled current densities are combined to yield the total current density as the sum of reciprocals:

$$\frac{1}{j} = \frac{1}{j_k} + \frac{1}{B\omega^{1/2}} \quad (1)$$

where  $j_k$  is activation controlled current density and  $B\omega^{1/2}$  is limiting current density that is linear function of the square root of the rotation rate.

From the Koutecky-Levich plots (Fig. 6b) (Eq. (1)) the kinetic currents of oxygen reduction is calculated from the intercepts of the  $1/j$  axis at  $1/\omega^{1/2} = 0$ . Experimentally obtained value of the constant  $B$  is found to be 0.022 mA rpm<sup>-1/2</sup>. This value is in a good agreement with the same already found in literature, for four-electron reduction of oxygen in 0.5 mol dm<sup>-3</sup> HClO<sub>4</sub>, at 25 °C [37]. The linearity and the parallelism of the plots indicate the first order kinetics with respect to molecular oxygen.

The Tafel plot for Nb-TiO<sub>2</sub>/Pt obtained from the kinetic currents is presented in Fig. 7. For comparison the Tafel plot for C/Pt is presented, as well. The both electrodes are characterized with two similar Tafel slopes close to -0.065 V dec<sup>-1</sup>, at low current densities, and -0.130 V dec<sup>-1</sup>, at high current densities suggesting the same mechanism of the reaction with the transition in the Tafel slope that is related, according to the literature [1,38,39], to the change in the nature of adsorbed oxygen containing species and their coverage variation with potential. In addition to blocking of the Pt sites, according to Markovic et al. [2] the adsorbed OH has an energetic effect on the kinetics of oxygen reduction, too, through

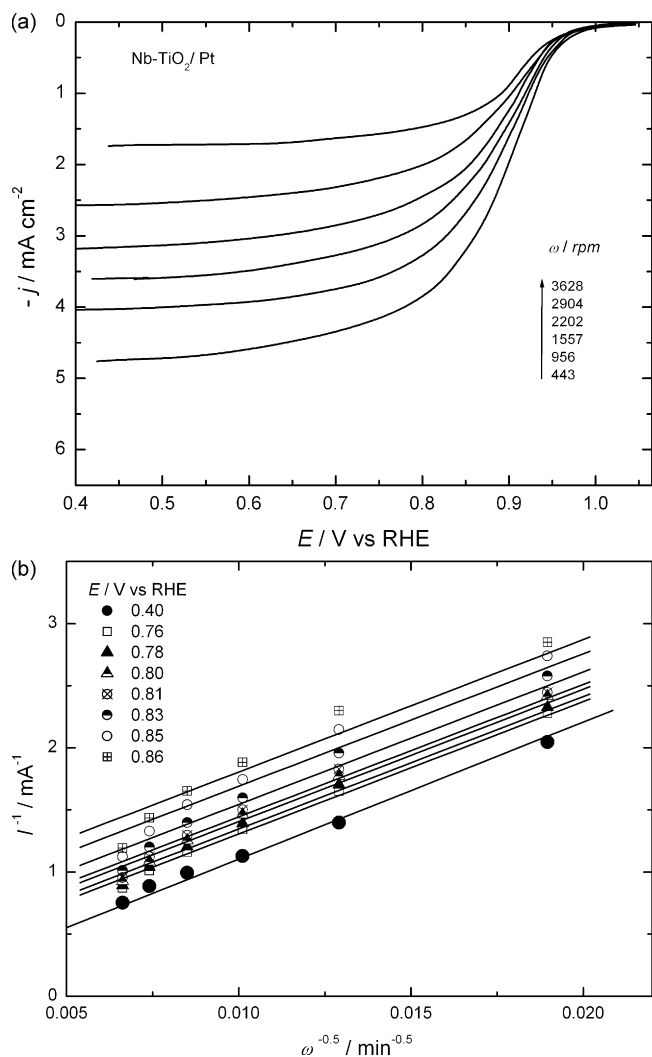


**Fig. 6.** Polarization curves (positive-going sweeps) obtained with rotating disk electrode for  $\text{O}_2$  reduction in  $0.5 \text{ mol dm}^{-3} \text{ HClO}_4$  solution, at Nb-TiO<sub>2</sub>/Pt ( $8 \mu\text{g}$ ) electrode. Current densities are based on the geometric surface area.

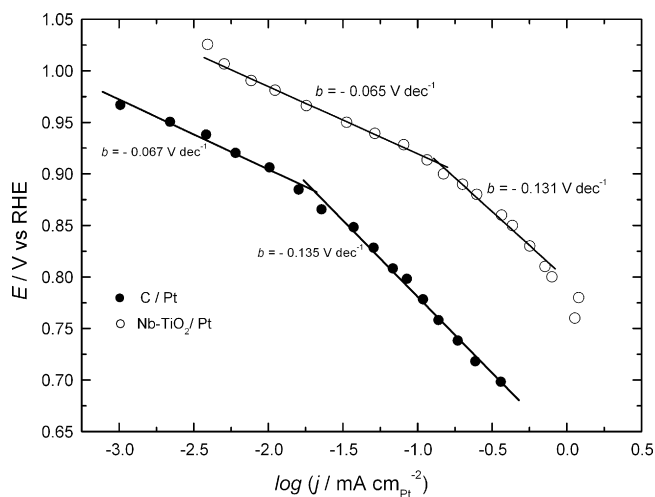


**Fig. 7.** Tafel plots normalized to the electrochemically active surface area for  $\text{O}_2$  reduction in  $0.5 \text{ mol dm}^{-3} \text{ HClO}_4$  solution at C/Pt and Nb-TiO<sub>2</sub>/Pt electrodes.

the change of Gibbs energy of adsorption of oxygen reduction intermediates by adsorbed OH. The both Tafel plots are normalized to the electrochemically active surface area and one could clearly see that the difference in activity expressed through the value of the current density at the constant potential is remarkable.

In order to compare catalytic activities of these catalysts specific and mass specific activities were evaluated at 0.85 and 0.90 V(RHE) where influences of mass transport are negligible (Table 1). The results show more than 10 times enhancement in oxygen reduction activity for Nb-TiO<sub>2</sub>/Pt catalyst.

The significant shift of PtOH formation to more positive potentials, facilitates the interaction of  $\text{O}_2$  with Pt increasing activity of the catalyst for oxygen reduction reaction. This obvious change of oxygen adsorption conditions, through the change of electronic structure of the catalyst, connected to the electronic interactions between platinum and the supportive material could be explained through the increase of 5d vacancy of Pt and decrease of Pt- $\text{O}$  bond distances. According to density functional calculations of adsorption energies and activation barriers the reactivity of metal atom is determined by the location of the centre of the local d-bond relative to the Fermium level [20,40]. Generally, the change in the surface d-state induces changes in the interaction between the adsorbate valence states and the metal surface.

The contractions of the Pt-Pt bonds and that effect to the inhibition of OH hemisorption on the Pt relating to the reduction of oxygen on Pt alloyed with the transition metals such as Cr, Si, V or Ti was suggested in the literature [41,42], as well.

One can find in the literature different specific activity data for Pt/C electrode [14,24,27,28]. That is why we used our Pt/C data for comparison to be sure that we are following the same experimental and calculation procedure (the same Nafion mass on the disc electrode, the same temperature and solution).

According to the results presented in the review paper of Gasteiger et al. [28], where they listed the activities for different Pt/C catalysts, whose surface areas were  $>60 \text{ m}^2 \text{ g}^{-1}_{\text{Pt}}$  we checked our results. Their values of  $i_{(0.9\text{V})} > 200 \mu\text{A cm}^{-2}_{\text{Pt}}$  are reported for the temperature between 65 and 80 °C while we gave value for 25 °C. So, taking into account literature reported value for the apparent enthalpy of activation, for ORR, in the low current density region of  $60 \text{ kJ mol}^{-1}$ , or in the high current density region of  $41 \text{ kJ mol}^{-1}$  [29,30], we calculated that specific activity for our Pt/C catalyst at 0.90 V for the temperature of 80 °C should be 274 or  $256 \mu\text{A cm}^{-2}_{\text{Pt}}$ , respectively, which is in a good agreement with listed results.

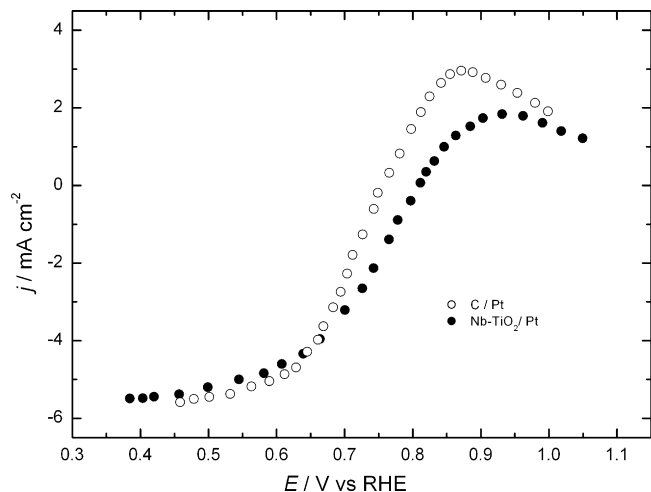
At the other hand, Mayrhofer et al. [14] reported their results that specific activities of Pt/C catalyst at 0.9 V are almost the same at 25 and 60 °C, as a result of very small energy of activation at constant cell voltage. So, according to their findings, the value that we used as a benchmark activity of Pt/C is significantly lower meaning that the catalytic activity of Nb-TiO<sub>2</sub>/Pt catalyst is lower, as well.

### 3.5. Oxygen reduction on Nb-TiO<sub>2</sub>/Pt catalyst in the presence of methanol

As the crossover of methanol from the anode to the cathode compartment leads to comparative reaction between reduction of oxygen and oxidation of methanol the sensitivity of the Nb-TiO<sub>2</sub>/Pt catalyst to the presence of methanol was checked by analysing  $j$ - $E$  polarization curves for methanol oxidation and oxygen reduction at the rotating speed of rpm with scan rate of  $20 \text{ mV s}^{-1}$ , in  $0.5 \text{ mol dm}^{-3} \text{ HClO}_4$  with  $0.1 \text{ mol dm}^{-3} \text{ MeOH}$  were done (Fig. 8). For comparison, the same voltammetric response for C/Pt was presented, too. For both catalysts the oxygen reduction is diffusion limited at  $E < 0.60 \text{ V(RHE)}$  and the limiting current densities are the same to those obtained in methanol-free electrolyte. As this value is consistent with four-electron process it proves that complete

**Table 1**Kinetic parameters for the oxygen reduction reaction obtained in 0.5 M HClO<sub>4</sub> at 25 °C for C/Pt, and Nb–TiO<sub>2</sub>/Pt catalysts.

Catalyst	Electrochem. active surface area (m <sup>2</sup> g <sup>-1</sup> Pt)	Tafel slope (mV dec <sup>-1</sup> )	Mass activity (mA mg <sup>-1</sup> Pt) at E/V vs. RHE		Specific activity (mA cm <sup>-2</sup> Pt) at E/V vs. RHE 0.85	
			0.85	0.90	0.85	0.90
			C/Pt	96	–67	33
Nb–TiO <sub>2</sub> /Pt	42.5	–65	172	70	0.405	0.165

**Fig. 8.** Voltammetric responses (positive-going sweeps) for Nb–TiO<sub>2</sub>/Pt and C/Pt electrode in 0.5 mol dm<sup>-3</sup> HClO<sub>4</sub> with 0.1 mol dm<sup>-3</sup> MeOH saturated with O<sub>2</sub>. Current densities are based on the geometric surface area.

reduction of oxygen to water occurs in the presence of methanol, as well. In the mixed kinetic-diffusion control region the potential loss with respect to oxygen reduction is about 50 mV lower at Nb–TiO<sub>2</sub>/Pt than at C/Pt which makes Nb–TiO<sub>2</sub>/Pt less affected by the presence of methanol. Meanwhile, the current density of methanol oxidation in oxygen saturated solution on Nb–TiO<sub>2</sub>/Pt at high potentials ( $E > 0.8$  V(RHE)) is lower than that on C/Pt suggesting that less active sites for oxygen reduction are blocked by methanol molecules or intermediates from methanol oxidation. The lower methanol coverage may be caused by the effect of the Pt particle shape on the distribution of the methanol adsorption [43] site or by the stronger adsorption of oxygenated species [44]. These results for methanol-tolerant OOR are comparable with the results obtained at Pt–Ni and Pt–Cr alloy catalysts [45,46].

#### 4. Conclusions

Nb-doped TiO<sub>2</sub> nanosized catalyst support with high specific surface area (72 m<sup>2</sup> g<sup>-1</sup>) is successfully synthesized through modified sol–gel procedure, avoiding carbon corrosion reaction that is disadvantage of carbon or very low specific surface area (15 m<sup>2</sup> g<sup>-1</sup>) that is disadvantage of sub-stoichiometric titanium oxides as supporting material.

The Nb–TiO<sub>2</sub> supported Pt (20 wt.%) uniformly distributed catalyst (Nb–TiO<sub>2</sub>/Pt) was prepared by means of borohydride reduction method.

The synthesized catalyst, in comparison with Pt carbon-supported one, shows the enhancement of the catalytic activity towards oxygen reduction that is very evident through the enhancement in oxygen reduction activity expressed through the specific current densities obtained at the constant potential. The reason for this is the interplay of the electronic and geometric factors and facilitation of O<sub>2</sub> interactions with the adsorption sites (so-called active sites) on the surface of the Nb–TiO<sub>2</sub>/Pt catalyst.

The four-electron reduction and the first charge transfer rate-determining step are operative in the whole range of potential.

Pt particles supported on Nb–TiO<sub>2</sub> powder are more efficient oxygen reduction catalyst in methanol-containing electrolyte, than the same supported on carbon, as the reason of Pt particle shape effect on the distribution of the methanol adsorption site or by the stronger adsorption of oxygenated species.

#### Acknowledgments

This work is financially supported by the Ministry of Science and Technological Development, Republic of Serbia, under Contract No. 142038. V. Radmilović acknowledges support by the US Department of Energy under Contract #DE-AC02-05CH11231.

#### References

- [1] A. Damjanovic, D.B. Sepa, *Electrochim. Acta* 35 (1990) 1157–1162.
- [2] N.M. Markovic, H.A. Gasteiger, P.N. Ross, *J. Phys. Chem.* 100 (1996) 6715–6721.
- [3] B. Gurau, E.S. Smotkin, *J. Power Sources* 112 (2002) 339–352.
- [4] T. Toda, H. Igarashi, H. Uchida, M. Watanabe, *J. Electrochem. Soc.* 146 (1999) 3750–3756.
- [5] M.T. Peffert, J.G. Beery, S. Gottesfeld, *J. Electrochem. Soc.* 135 (1988) 1431–1436.
- [6] M.T. Paffet, K.A. Daube, S. Gottesfeld, T.C. Campbell, *J. Electroanal. Chem.* 220 (1987) 269–285.
- [7] J. Liu, J. Cao, Q. Huang, X. Li, Z. Zou, H. Yang, *J. Power Sources* 175 (2008) 159–165.
- [8] J.S. Cooper, P.J. McGinn, *J. Power Sources* 163 (2006) 330–338.
- [9] C. Roth, M. Goetz, H. Fuess, *J. Appl. Electrochem.* 31 (2001) 793–798.
- [10] W.C. Choi, J.D. Kim, S.I. Woo, *Catal. Today* 74 (2002) 235–240.
- [11] J. Zhang, M.B. Vukmirovic, K. Sasaki, A.U. Nilekar, M. Mavrikakis, R. Adzic, *J. Am. Chem. Soc.* 127 (2005) 12480–12481.
- [12] M. Min, J. Cho, K. Cho, K. Him, *Electrochim. Acta* 45 (2000) 4211–4217.
- [13] J. Cho, W. Roh, D. Kim, J. Yoon, J. Choy, H. Kim, *J. Chem. Soc., Faraday Trans. 94* (1998) 2835–2841.
- [14] K.J.J. Mayrhofer, D. Strmcnik, B.B. Blizanac, V. Stamenkovic, M. Arenz, N.M. Markovic, *Electrochim. Acta* 53 (2008) 3181–3188.
- [15] C.A. Reiser, L. Bregoli, T.W. Patterson, S.Yi, Jung, J.D. Yang, M.L. Perry, T.D. Jarvi, *Electrochem. Solid-State Lett.* 8 (2005) A273–A276.
- [16] G.R. Dieckmann, S.H. Langer, *Electrochim. Acta* 44 (1998) 437–444.
- [17] L. He, H.F. Franzen, J.E. Vitt, D.C. Johnson, *J. Appl. Electrochem.* 26 (1996) 785–793.
- [18] E.E. Farndon, D. Pletcher, *Electrochim. Acta* 42 (1997) 1281–1285.
- [19] L. Brewer, P.R. Wengert, *Metal Trans.* 4 (1973) 83–104.
- [20] B. Hammer, J.K. Norskov, *Adv. Catal.* 45 (2000) 71–129.
- [21] L.M. Vračar, N.V. Krstajić, M.M. Jakšić, V.R. Radmilović, *J. Electroanal. Chem.* 587 (2006) 99–107.
- [22] K. Sasaki, L. Zhang, R.R. Adzic, *Phys. Chem. Chem. Phys.* 10 (2008) 159–167.
- [23] R.K. Sharma, M.C. Bhatnagar, G.L. Sharma, *Appl. Surf. Sci.* 92 (1996) 647–650.
- [24] G. Chen, S.R. Bare, T.E. Mallouk, *J. Electrochem. Soc.* 149 (2002) A1092–A1099.
- [25] K.W. Park, K.S. Seul, *Electrochem. Commun.* 9 (2007) 2256–2260.
- [26] A.M. Ruiz, G. Dezanneau, J. Arbiol, A. Cornet, J.R. Morante, *Chem. Mater.* 16 (2004) 862–871.
- [27] U.A. Paulus, T.J. Schmidt, H.A. Gasteiger, R.J. Behm, *J. Electroanal. Chem.* 495 (2001) 134–135.
- [28] H.A. Gasteiger, S.S. Kocha, B. Sompalli, F.T. Wagner, *Appl. Catal. B: Environ.* 56 (2005) 9–35.
- [29] N. Wakabayashi, M. Takeichi, H. Uchida, M. Watanabe, *J. Phys. Chem. B* 109 (2005) 5836.
- [30] N. Wakabayashi, M. Takeichi, M. Itagaki, H. Uchida, M. Watanabe, *J. Electroanal. Chem.* 574 (2005) 339.
- [31] S. Boujdaj, F. Wunsch, P. Portes, J.F. Bocquet, C. Colbeau-Justin, *Sol. Energy Mater. Sol. Cells* 83 (2004) 421–423.
- [32] B. Babic, B. Kaludjerovic, Lj.M. Vracar, N. Krstajic, *Carbon* 42 (2004) 2617–2624.
- [33] B.M. Babic, Lj.M. Vracar, V. Radmilovic, N.V. Krstajic, *Electrochim. Acta* 51 (2006) 3820–3826.
- [34] E.P. Barret, L.G. Joyner, P.P. Halenda, *J. Am. Chem. Soc.* 73 (1951) 373–380.
- [35] K.S.W. Sing, D.H. Everett, R.A.W. Haul, L. Moscou, R.A. Pierotti, J. Rouquerol, T. Siemieniowska, *Pure Appl. Chem.* 57 (1985) 603–619.
- [36] J.T. Hwang, J.S. Chung, *Electrochim. Acta* 38 (1993) 2715–2723.

- [37] M.H. Lee, J.S. Do, J. Power Sources 188 (2009) 353–358.
- [38] B.B. Sepa, M.V. Vojnovic, Lj. Vracar, A. Damjanovic, Electrochim. Acta 31 (1986) 91–96.
- [39] A. Damjanovic, A. Dey, J.O.M. Bockris, Electrochim. Acta 11 (1966) 791–814.
- [40] A. Ruban, B. Hammer, P. Stoltze, H.L. Skriver, J.K. Norkov, J. Mol. Catal. A 115 (1997) 421–429.
- [41] S. Mukerjee, S. Srinivasan, M. Soriaga, J. Mc Breen, J. Phys. Chem. 99 (1995) 4577–4589.
- [42] S. Mukerjee, J. Appl. Electrochem. 20 (1990) 537–548.
- [43] T. Frelink, W. Visscher, J.A.R. vanVeen, J. Electroanal. Chem. 382 (1995) 65–72.
- [44] S. Mukerjee, J. McBreen, J. Electroanal. Chem. 448 (1998) 163–171.
- [45] H. Yang, N. Alonso-Vante, J.-M. Leger, C. Lamy, J. Phys. Chem. B 108 (2004) 1938–1947.
- [46] H. Yang, C. Coutanceau, J.-M. Leger, N. Alonso-Vante, C. Lamy, J. Electroanal. Chem. 576 (2005) 305–313.